Enhanced Superconductivity in Monolayer T_d-MoTe$_2$

Daniel A. Rhodes,*[◆] Apoorv Jindal,[◆] Noah F. Q. Yuan, Younghun Jung, Abhinandan Antony, Hua Wang, Bumho Kim, Yu-che Chiu, Takashi Taniguchi, Kenji Watanabe, Katayun Barmak, Luis Balicas, Cory R. Dean, Xiaofeng Qian, Liang Fu, Abhay N. Pasupathy,* and James Hone*

Cite This: https://dx.doi.org/10.1021/acs.nanolett.0c04935

Read Online

ACCESS | Metrics & More | Article Recommendations | SI Supporting Information

ABSTRACT: Crystalline two-dimensional (2D) superconductors (SCs) with low carrier density are an exciting new class of materials in which electrostatic gating can tune superconductivity, electronic interactions play a prominent role, and electrical transport properties may directly reflect the topology of the Fermi surface. Here, we report the dramatic enhancement of superconductivity with decreasing thickness in semimetallic T_d-MoTe$_2$, with critical temperature (T_c) increasing up to 7.6 K for monolayers, a 60-fold increase with respect to the bulk T_c. We show that monolayers possess a similar electronic structure and density of states (DOS) as the bulk, implying that electronic interactions play a strong role in the enhanced super-conductivity. Reflecting the low carrier density, the critical temper-

ature, magnetic field, and current density are all tunable by an applied gate voltage. The response to high in-plane magnetic fields is distinct from that of other 2D SCs and reflects the canted spin texture of the electron pockets.

KEYWORDS: 2D Superconductivity, Weyl semimetal, Two-dimensional materials, gate-tunable
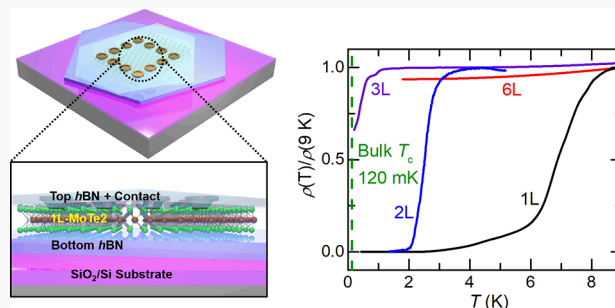
In the 2D limit, superconductivity can differ strongly from the bulk due to spatial confinement and increased interactions and can be tuned electrostatically, opening up new possibilities for device applications.[1] 2D superconductivity has been extensively studied in metallic and metal-oxide films. In these systems, disorder plays a strong role, and interaction with the substrate or capping layers via strain or charge transfer can strongly alter the superconducting behavior.[1−3] Recently, exfoliated 2D metallic superconductors (SCs) such as NbSe$_2$[4] and TaS$_2$[5] as well as 2D semiconductors (e.g., MoS$_2$) with high induced carrier densities through ionic liquid gating,[6] have provided new opportunities to study 2D superconductivity in crystalline systems with weak substrate interaction. This has resulted in the observation of new phenomena, such as enhanced upper critical fields from strong out-of-plane spin−orbit coupling (SOC), enhanced T_c as one approaches the monolayer limit,[7] and the electrostatic control over the dissipation of vortices.[8] Very recently, superconductivity has been discovered in twisted bilayer graphene (T_c = 2 K) and monolayer T_d-WTe$_2$ (T_c = 700 mK), at low carrier densities ($<10^{13}$/cm^2 induced by an electrostatic gate).[9−11] The strong carrier−carrier interactions and facile tuning by conventional gates in this regime have generated intense interest, motivating the search for additional low-density 2D SCs.

Here, we explore the superconducting properties of T_d-MoTe$_2$ in the 2D limit. Bulk T_d-MoTe$_2$ is a type-II Weyl semimetal[12] with a carrier density of 6×10^{19} cm^{-3},[13] and a T_c of 120 mK, which can be enhanced by doping or applied

pressure.[14,15] To date, no work has explored T_d-MoTe$_2$ in its intrinsic 2D limit: few-layer films grown by chemical vapor deposition (CVD) exhibit superconductivity with T_c up to 3 K but are highly doped, with carrier densities of $\sim 3 \times 10^{14}$/cm^2, and show no superconductivity for films thinner than 2 nm.[16,17]

In this study, we utilize high-quality single crystals synthesized by a self-flux technique; recent studies indicate that this high quality is maintained after mechanical exfoliation.[23] Thin flakes were exfoliated inside a nitrogen glovebox and encapsulated in hexagonal boron nitride (hBN) crystals to reduce environmental disorder and provide protection from degradation in air.[24] Hermetically sealed electrical contacts were obtained by embedding metal electrodes within the hBN[25] or by encapsulating prepatterned contacts (Section 2b in the Supporting Information). As we detail below, this approach maintains intrinsic low carrier density and allows us to access the clean limit, where the normal-state mean free path exceeds the superconducting coherence length.
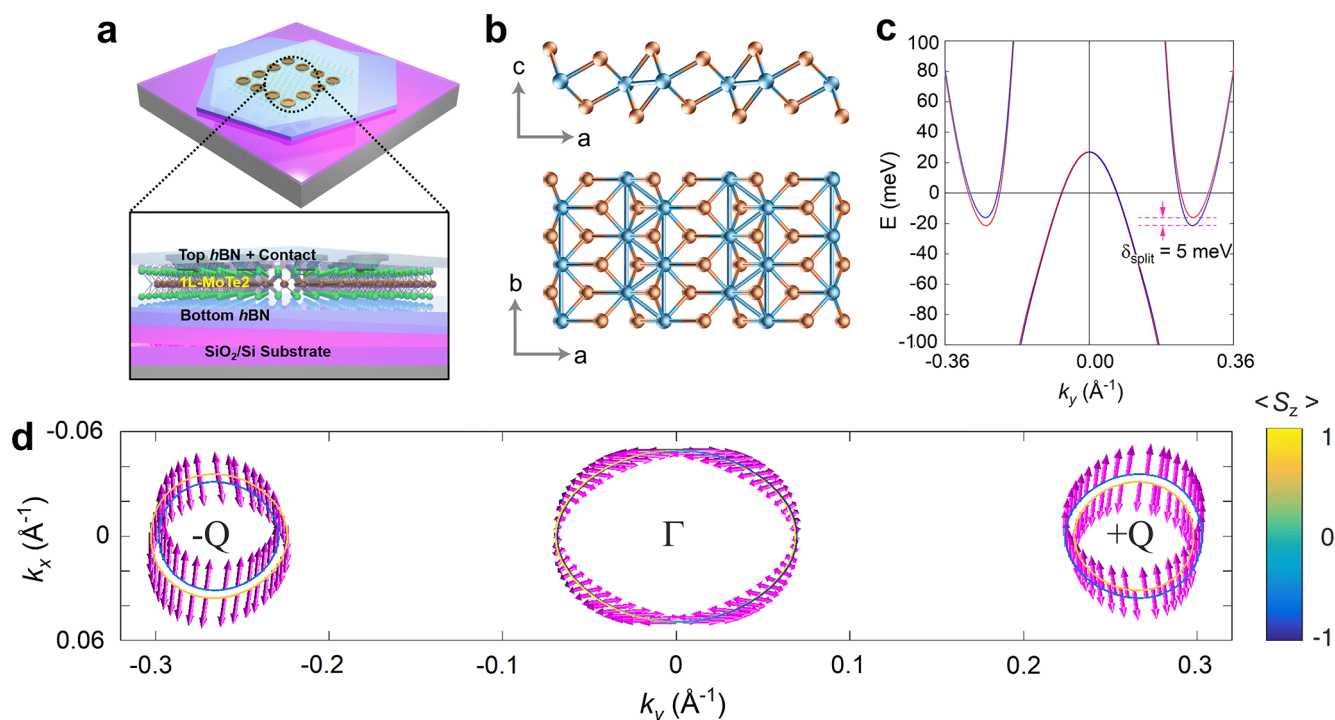
Figure 1. (a) Device schematic. (b) Crystal structure for 1L-MoTe$_2$. Blue atoms depict Mo and red atoms Te. (c) Density-functional theory (DFT) calculations for its electronic band structure. (d) Calculated spin texture, with the spin orientation indicated by arrows. Color scale indicates out-of-plane direction.
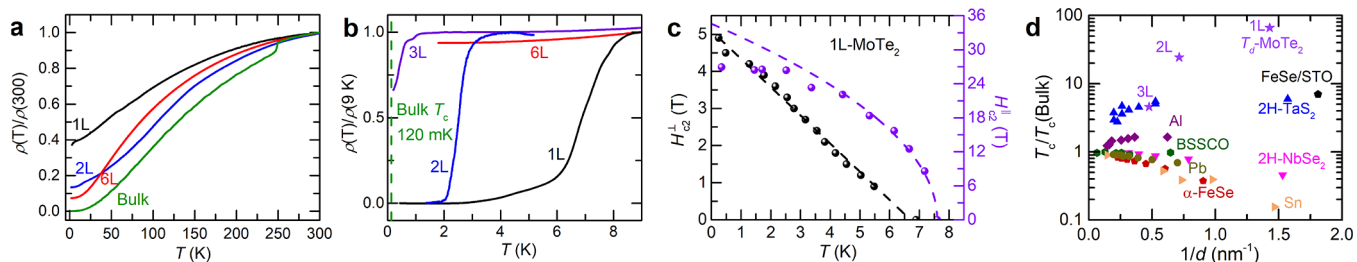

Figure 2. (a, b) Normalized resistivity as a function of temperature T for various layer numbers. The vertical dashed line indicates T_c for bulk T_d-MoTe$_2$. (c) Temperature dependence of $H_{c2}^\perp$ and $H_{c2}^\parallel$ for sample S2. Dashed lines are fits to GL theory. (d) T_c as a function of the inverse sample thickness, $1/d$, in T_d-MoTe$_2$, BSCCO,[18,19] α-FeSe,[2] FeSe on STO,[3] Sn,[20] Al,[21] Pb,[22] 2H-TaS$_2$,[5] and 2H-NbSe$_2$.[4]

Monolayer T_d-MoTe$_2$ (1L-MoTe$_2$) is isostructural to 1L-WTe$_2$ (Figure 1b). Previous studies have shown that bulk crystals transition to the T_d phase upon cooling below 240 K,[26] whereas for thin samples the T_d phase has been observed above room temperature.[27] We note that the T' and T_d phases differ in interlayer stacking, but their monolayers are identical. Figure 1b shows the calculated electronic band structure, with one hole pocket at the Γ point (carrier density $n = 1.2 \times 10^{13}$/cm^2) and two electron pockets ($n = 0.6 \times 10^{13}$/cm^2) at either side of the Γ point, denoted as $\pm Q$. With a small out-of-plane electric field, inversion symmetry is broken, and significant SOC develops.[28] For this reason, and in reasonable agreement with our data as discussed below, the band structure was calculated under the assumption of an applied, out-of-plane electric field of 0.1 V/nm. With this SOC, the Γ pocket is nearly spin degenerate, and the $\pm Q$ pockets exhibit a spin-splitting of $\sim$5 meV.

In both pockets, the spins are tilted rather than being entirely locked along the out-of-plane direction as in the 2H-phase, e.g., NbSe$_2$. For the Γ pocket, the spin orientation depends strongly on momentum orientation, while for the $\pm Q$

pockets the spins are tilted in the toward the b-axis, independent of the momentum (Figure 1c). However, conclusive experimental confirmation of this band structure is lacking. One report indicates a potential band gap in few-layered T_d-MoTe$_2$,[29] while two recent angle-resolved photo-emission spectroscopy (ARPES) studies on 1L-MoTe$_2$ show conflicting results: semimetallic behavior with large band overlap for 1L-MoTe$_2$ grown on graphene,[30] and a weak overlap with a potential gap opening for 1L-MoTe$_2$ exfoliated on gold.[31] To this end, in this paper, we seek to shed light on the electronic band structure of 1L-MoTe$_2$ through magneto-transport measurements.

Figure 2a shows the temperature-dependent resistivity for a typical bulk crystal and samples composed of 1, 2, 3, and 6 layers. Bulk single crystals show metallic behavior with a residual resistance ratio (RRR) as large as 2000, an improvement of almost 2 orders of magnitude with respect to recent reports,[15] attesting to the high sample quality. Bulk samples also show the expected $T'-T_d$ phase transition at 240 K, whereas the monolayer (1L), 2L, and 6L samples do not. This is consistent with previous studies indicating that the T_d
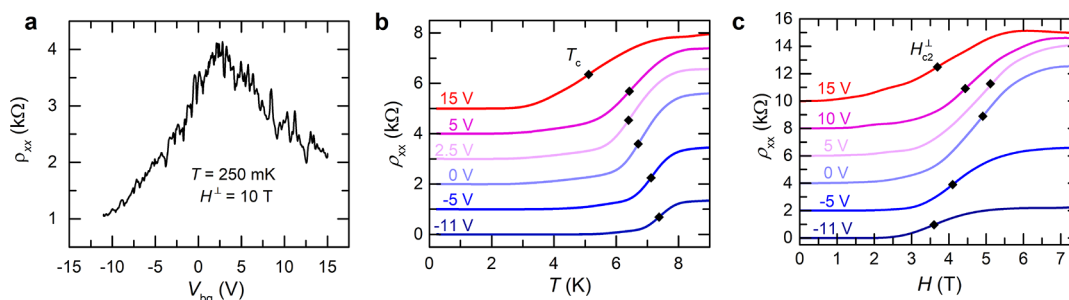
Figure 3. (a) Normal state resistance, ρ_{xx} as a function of back-gate voltage, V_{bg} ($H^{\perp} = 10$ T). Note that, from the thickness and dielectric constant of hBN, the estimated induced carrier density is $0.5 \times 10^{12}/\text{cm}^2$ per applied volt. (b, c) Temperature and magnetic field dependence of ρ_{xx} for $V_{bg} = -11$ to 15 V, respectively. All curves are vertically displaced by (b) 1 kΩ and (c) 2 kΩ for clarity. Diamond markers indicate T_c and $H_{c2}^{\perp}$ for $\rho_{xx} = 50\%$ of the normal state resistance, respectively.

phase persists to above room temperature[27] in the few-layer limit. In agreement with the calculated band structure, nearly intrinsic, as we will show later, few-layer samples remain metallic down to low temperature, ruling out the presence of a band gap.[32]

The central result of this paper is shown in Figure 2b. Upon cooling, 1L, 2L, and 3L T_d-MoTe$_2$ show a strong enhancement of the T_c when compared to the bulk T_c. For the monolayer, an onset T_c of 7.6 K is observed, almost 2 orders of magnitude larger than the bulk T_c. In contrast, the 2L and 3L samples exhibit a T_c of 2.5 and ~0.5 K, respectively. The 6L sample shows no superconducting behavior down to 20 mK (Figure S4 in the Supporting Information).

Next, we characterize the superconducting phase diagram of the monolayer under applied magnetic fields. Figure 2c shows the measured perpendicular ($H_{c2}^{\perp}$) and parallel ($H_{c2}^{\parallel}$) critical fields as a function of temperature relative to the ab-plane, defined at 50% of the normal-state resistivity. $H_{c2}^{\perp}$ reaches 5 T at 0 K and decreases linearly with increasing temperature, consistent with the 2D Ginzburg–Landau (GL) equation for fields out of the plane: $\mu_0 H_{c2}^{\perp} = \frac{\Phi_0}{2\pi\xi_0^2}(1 - T/T_c)$, where Φ_0 is the flux quantum, μ_0 the permeability of free space, and ξ_0 the in-plane coherence length.[33] A linear fit (solid line) yields $\xi_0 = 8.03$ nm (8.1 nm for $\mu_0 H_{c2}^{\perp} = \frac{\Phi_0}{2\pi\xi_0^2}$ at 250 mK), roughly one-third of the bulk coherence length.[34] This value is on the order of the electronic mean free path, $l \sim 6$ nm (Section 3 and Table S1 of the Supporting Information). Therefore, whereas recent studies on 1L-WTe$_2$ were performed in the dirty limit ($\xi_0 \gg l$),[10,11] in this work we explore superconductivity in the regime where the effects of spin–orbit scattering (SOS) on the superconductivity can be ignored. At fields up to 20 T, $H_{c2}^{\parallel}$ follows a square root temperature dependence with a critical field well beyond the Pauli limit ($H_p = 1.84T_c = 14$ T), consistent with other 2D SCs characterized by strong SOC such as NbSe$_2$.[4]

A number of factors indicate that these samples are close to charge compensation (as depicted in Figure 1c), distinguishing this study from previous reports of enhanced superconductivity in CVD-grown few-layer MoTe$_2$ at high ($\sim 3 \times 10^{14}/\text{cm}^2$) levels of defect-induced doping.[16] The high RRR of the bulk crystal indicates much lower defect density than in the CVD-grown films. While it is possible that additional defects could be introduced as a result of oxidation during processing, we have found that devices assembled in an atmosphere with greater than a few ppm of oxygen are not superconducting. The normal-state resistivity shows a peak near zero back-gate

voltage (Figure 3a) and displays superlinear magnetoresistance (Figure S5c in thSupporting Information), both of which are consistent with charge compensation. Likewise, the small and gate-tunable Hall coefficient (Figure S5b in the Supporting Information) is consistent with charge compensation in a semiclassical two-band model,[35] whereas a single-band model gives unphysically large carrier density and is inconsistent with the observed gate-tuning. Additionally, we have observed Shubnikov−de Haas (SdH) oscillations in 2L and 3L samples which also indicate a carrier density of ~$2 \times 10^{13}/\text{cm}^2$ per layer (Figure S6 in the Supporting Information). From these observations, we conclude that 1L-MoTe$_2$ shows a large enhancement of T_c while maintaining a carrier density and DOS to similar to those of the bulk.

In conventional SCs many factors tend to suppress superconductivity in the 2D limit. GL theory predicts the suppression of superconductivity for films with thicknesses smaller than the bulk coherence length,[36] as seen in other crystalline 2D SCs (e.g., $2H$-NbSe$_2$[4] and few-layer FeSe on bilayer graphene[2]). In addition, repulsive electron−electron interactions, represented by the screened Coulomb pseudo-potential μ^* in Eliashberg theory, increase as materials approach the 2D limit and lead to suppression of T_c by decreasing the effective pairing interaction.[37] Thus, the suppression of superconductivity in 6L-MoTe$_2$ represent the expected result, whereas its enhancement in 1L, 2L, and 3L samples is surprising. In fact, enhancement of T_c in the 2D limit (without doping or other extrinsic factors) is extremely rare, with a few prominent examples shown in Figure 2d. For the most notable example, monolayer FeSe grown on strontium titanate (STO),[3,38] the mechanism for enhancement is not yet understood but clearly requires strong substrate interaction, since the opposite trend is observed for FeSe on weakly interacting substrates.[2] $2H$-TaS$_2$ shows increasing T_c for thicknesses below the coherence length,[5] with 4-fold enhancement in T_c for the monolayer.[7] Potential mechanisms include an increase in the DOS via suppression of a competing charge-density wave,[39] decreased interlayer coupling,[5] and the formation of a second superconducting band.[7] As noted above, the closest parallels to the present case are twisted bilayer graphene and monolayer WTe$_2$, which show superconductivity not found in the bulk when carrier density is appropriately tuned with an external gate.

The observed enhancement in T_c in 1L-MoTe$_2$, which occurs without substantial changes to carrier density or DOS, does not seem to be consistent with phonon-mediated superconductivity. No significant changes are observed in the

vibrational frequencies or the electron−phonon coupling through Raman spectra[40,41] and DFT calculations[42] between the bulk and monolayer limit. This enhancement must therefore come from an increase in the pairing interaction. There is already significant evidence that superconductivity in bulk T_d-MoTe$_2$ is electronically mediated,[34,43,44] and as discussed above, μ^* is expected to be largest for monolayers. Hence, we postulate that the change in the Coulomb interaction with dimensionality may account for the enhancement in T_c via spin fluctuations, although more work is necessary to conclusively establish the superconducting mechanism.

Given the low carrier density of 1L-MoTe$_2$, it is interesting to examine the gate-tunability of superconductivity. Figure 3b,c shows the gate-tunability of the superconducting transition as a function of the temperature (Figure 3b) and out-of-plane magnetic fields (Figure 3c). As shown, T_c increases uniformly with net carrier density, varying from ∼5 in the electron dominated region up to ∼8 K in the hole dominated region. In contrast, H_{c2} peaks concurrently with the normal-state resistivity (Figure 3a). The reason for the different gate-dependence of T_c and H_{c2} is unclear but may be related to variations in the mean free path and/or coherence length near neutrality, such that the system moves toward the dirty limit.[33] Finally, we note that for all measured samples the superconducting transition broadens with electron doping. Direct probes of the crystal structure or electronic band structure at low temperatures (e.g., using Raman spectroscopy or ARPES) with gating may shed light on the origin of this effect.

Finally, we turn our attention to the enhanced $H_{c2}^{\parallel}$, its deviation from GL theory, and its relationship to the overall spin texture. The spin texture is determined by the momentum-dependent SOC vector, $\mathbf{g_k}$. At the Γ point, $\mathbf{g_k}$ must vanish (to leading order in momentum) under time-reversal symmetry due to its odd parity, and higher-order effects lead to a strongly momentum-dependent spin texture for T_d-MoTe$_2$ (Figure 1c). On the other hand, at non-time-reversal-invariant points, the SOC vector becomes a nonzero constant Zeeman field, denoted as $\mathbf{g}$, which couples to only one component of the electron spin and is independent of momentum. To recover overall time-reversal symmetry, at the time-reversal partner $-\mathbf{k}$, the SOC vector becomes $-\mathbf{g}$. This is known as Ising SOC,[4−6] where the overall spin texture resulting from this SOC is determined by the point group symmetry. In the 2H-TMDs, the Ising SOC vector is perpendicular to the plane. In contrast, 1L-MoTe$_2$ has an Ising SOC vector which is *tilted* with respect to the out-of-plane direction (Figure 1a), giving a polar angle of ∼45° due to the low symmetry at the Q points.[28]

The in-plane field response of 2H-TMDs is well described by a linearized gap equation which takes into account the out-of-plane SOC,[4,5] resulting in a square-root temperature dependence $H_{c2}^{\parallel}(T) = H_0(1 - T_c/T_{c0})^{1/2}$ akin to GL theory,[4] and value of H_0 far exceeding the Pauli limit. Here, we extend this theory to a two-component spin−orbit coupling vector. Given an in-plane magnetic field $\mathbf{H} = H(\cos \phi, \sin \phi, 0)$, we compute $\Delta_{so}^{\parallel} = \mathbf{g} \cdot \hat{\mathbf{H}}$ and $\Delta_{so}^{\perp} = |\mathbf{g} \times \hat{\mathbf{H}}|$, with both depending on the in-plane angular direction, ϕ, of the applied magnetic field (Section 4 in the Supporting Information). With the spin tilted at 45°, the ratio $|\Delta_{so}^{\parallel}/\Delta_{so}^{\perp}|$ can vary from 0 to 1, depending on ϕ. For $\phi = 0$ and π, $|\Delta_{so}^{\parallel}/\Delta_{so}^{\perp}| \sim 0$, and the behavior is identical to that of the 2H-TMDs. In contrast, when $|\Delta_{so}^{\parallel}/\Delta_{so}^{\perp}| \neq 0$, the solution to this linearized gap equation is instead a digamma

function (Section 4 and Figure S8a in the Supporting Information), where $H_{c2}^{\parallel}(T)$ exhibits a peak as T approaches 0 K.

Figure 4a,b shows the measured $H_{c2}^{\parallel}(T)$ for two different 2H-TMDs, NbSe$_2$ and TaS$_2$, and for T_d-MoTe$_2$. This data is
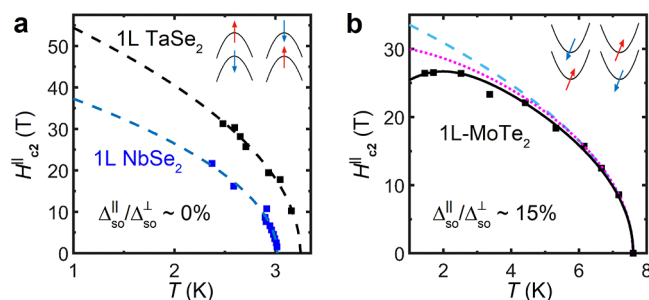
Figure 4. (a) Measured $H_{c2}^{\parallel}$ for fields parallel to the *ab*-plane in 1L 2H-TaS$_2$ and 2H-NbSe$_2$. (b) $H_{c2}^{\parallel}$ vs T_c for S1. The dotted magenta line is a fit to KLB theory. (a) Adapted from refs 4 and 5. Insets depict the spin texture of K/K′ and Q, −Q pockets, respectively.

fitted to the linearized gap equation, with $\Delta_{so}^{\parallel}$ and $\Delta_{so}^{\perp}$ as fitting parameters. In agreement with the expected outcome in prior reports,[4,45] $H_{c2}^{\parallel}$ for NbSe$_2$ and TaS$_2$ follows a square root temperature dependence over the entire measurable range and yields $\Delta_{so}^{\parallel} \sim 0$. For 1L-MoTe$_2$, the measured $H_{c2}^{\parallel}$ clearly falls below the square-root dependence at low T, and the two-component SOC model provides an excellent fit to the data over the entire field and temperature range. We find $\Delta_{so}^{\perp} \sim 2.34$ meV, with $\Delta_{so}^{\parallel}/\Delta_{so}^{\perp}$ between 13% and 17% (Section 4 and Figure S8 in the Supporting Information). We also note that the Klemm−Luther−Beasley (KLB) model, which applies to superconductivity in the dirty limit with strong SOS, overestimates $H_{c2}^{\parallel}$ at low temperatures. This is in agreement with estimations of the SOS time which indicate that our 1L-MoTe$_2$ samples do not meet the criteria for the dirty limit (Table S2 in the Supporting Information).

While the fit from the two-component SOC model to the critical field data is consistent with a tilted Ising spin texture, open issues remain. Most importantly, without knowledge of the sample orientation it is impossible to determine whether the extracted value $H_{c2}^{\parallel}/H_p$ accurately reflects the tilted spin texture. In addition, recently proposed models for the spin−orbit−parity coupling (SOPC) enhancement of H_{c2}[46] may also explain the observed behavior. The dominant mechanism for enhancement of H_{c2} between SOPC and SOC remains to be determined. Measurements of the upper critical fields as a function of ϕ will greatly help to clarify these issues. Finally, we note that all successfully fabricated devices show similar results, with measurements repeated in two 1L, three 2L, and three 3L samples.

The telluride family of TMDs remains poorly explored. Rich phenomena should emerge now that reliable and clean fabrication processes are available for the study of air-sensitive monolayers. Here, the demonstration of strongly enhanced, gate-tunable superconducting transitions in 1L-MoTe$_2$ should motivate future studies to understand the mechanism for the observed enhancement and to confirm the proposed tilted Ising SOC, which remains an experimental challenge due to the need for in-plane rotation in magnetic fields in excess of 25 T at low temperatures. Additionally, the electronic structure of MoTe$_2$ is highly sensitive to external factors like strain or

electric fields,[28,47−49] allowing study of how the superconducting phase may be modified by varying the SOC. Finally, we note that recent investigations into bulk T_d-MoTe$_2$ have revealed the existence of superconducting edge currents.[50] While this result remains to be shown in few-layer MoTe$_2$, electrostatic control over the charge carriers and much higher T_c when compared to that of the bulk could provide a unique platform for quantum logic devices based on topological protection.

■ ASSOCIATED CONTENT

ⓈⒾ Supporting Information

The Supporting Information is available free of charge at https://pubs.acs.org/doi/10.1021/acs.nanolett.0c04935.

> Description of crystal growth, fabrication methods, analysis of the electronic transport, description of DFT calculations, optical images of differing layer numbers, Hall measurements, nonlinear magnetoresistance, SdH oscillations in multilayer, and comparative fittings for the parallel upper critical fields (PDF)

■ AUTHOR INFORMATION

Corresponding Authors

Daniel A. Rhodes − *Department of Mechanical Engineering, Columbia University, New York 10027, United States; Department of Materials Science and Engineering, University of Wisconsin−Madison, Madison, Wisconsin 53706, United States;* ⓞ orcid.org/0000-0002-7651-3211; Email: darhodes@wisc.edu

Abhay N. Pasupathy − *Department of Physics, Columbia University, New York 10027, United States;* ⓞ orcid.org/0000-0002-2744-0634; Email: apn2108@columbia.edu

James Hone − *Department of Physics, Columbia University, New York 10027, United States;* Email: jh228@columbia.edu

Authors

Apoorv Jindal − *Department of Physics, Columbia University, New York 10027, United States*

Noah F. Q. Yuan − *Department of Physics, Massachusetts Institute of Technology, Cambridge, Massachusetts 02142, United States*

Younghun Jung − *Department of Mechanical Engineering, Columbia University, New York 10027, United States*

Abhinandan Antony − *Department of Mechanical Engineering, Columbia University, New York 10027, United States*

Hua Wang − *Department of Materials Science and Engineering, Texas A&M University, College Station, Texas 77840, United States*

Bumho Kim − *Department of Mechanical Engineering, Columbia University, New York 10027, United States*

Yu-che Chiu − *Department of Physics and National High Magnetic Field Laboratory, Florida State University, Tallahassee, Florida 32306, United States*

Takashi Taniguchi − *National Institute for Materials Science, Tsukuba 305-0044, Japan;* ⓞ orcid.org/0000-0002-1467-3105

Kenji Watanabe − *National Institute for Materials Science, Tsukuba 305-0044, Japan;* ⓞ orcid.org/0000-0003-3701-8119

Katayun Barmak − *Department of Applied Physics and Applied Mathematics, Columbia University, New York 10027, United States*

Luis Balicas − *Department of Physics and National High Magnetic Field Laboratory, Florida State University, Tallahassee, Florida 32306, United States;* ⓞ orcid.org/0000-0002-5209-0293

Cory R. Dean − *Department of Physics, Columbia University, New York 10027, United States*

Xiaofeng Qian − *Department of Materials Science and Engineering, Texas A&M University, College Station, Texas 77840, United States;* ⓞ orcid.org/0000-0003-1627-288X

Liang Fu − *Department of Physics, Massachusetts Institute of Technology, Cambridge, Massachusetts 02142, United States*

Complete contact information is available at:
https://pubs.acs.org/10.1021/acs.nanolett.0c04935

Author Contributions

◆D.A.R. and A.J. contributed equally.

Notes

The authors declare no competing financial interest.

■ ACKNOWLEDGMENTS

■ REFERENCES

(1) Saito, Y.; Nojima, T.; Iwasa, Y. Highly crystalline 2D superconductors. *Nature Reviews Materials* **2017**, *2*, 16094.

(2) Song, C.-L.; Wang, Y.-L.; Jiang, Y.-P.; Li, Z.; Wang, L.; He, K.; Chen, X.; Ma, X.-C.; Xue, Q.-K. Molecular-beam epitaxy and robust superconductivity of stoichiometric FeSe crystalline films on bilayer graphene. *Phys. Rev. B: Condens. Matter Mater. Phys.* **2011**, *84*, 020503.

(3) Huang, D.; Hoffman, J. E. Monolayer FeSe on SrTiO3. *Annu. Rev. Condens. Matter Phys.* **2017**, *8*, 311−336.

(4) Xi, X.; Wang, Z.; Zhao, W.; Park, J.-H.; Law, K. T.; Berger, H.; Forró, L.; Shan, J.; Mak, K. F. Ising pairing in superconducting NbSe$_2$ atomic layers. *Nat. Phys.* **2016**, *12*, 139−143.

(5) Barrera, S. C. d. l.; Sinko, M. R.; Gopalan, D. P.; Sivadas, N.; Seyler, K. L.; Watanabe, K.; Taniguchi, T.; Tsen, A. W.; Xu, X.; Xiao, D.; Hunt, B. M. Tuning Ising superconductivity with layer and spin-orbit coupling in two-dimensional transition-metal dichalcogenides. *Nat. Commun.* **2018**, *9*, 1427.

(6) Lu, J. M.; Zheliuk, O.; Leermakers, I.; Yuan, N. F. Q.; Zeitler, U.; Law, K. T.; Ye, J. T. Evidence for two-dimensional Ising super-conductivity in gated MoS2. *Science* **2015**, *350*, 1353−1357.

(7) Talantsev, E. F.; Crump, W. P.; Island, J. O.; Xing, Y.; Sun, Y.; Wang, J.; Tallon, J. L. On the origin of critical temperature enhancement in atomically thin superconductors. *2D Mater.* **2017**, *4*, 025072.

(8) Benyamini, A.; Kennes, D. M.; Telford, E. J.; Watanabe, K.; Taniguchi, T.; Millis, A. J.; Hone, J.; Dean, C. R.; Pasupathy, A. N. Nonmonotonic Temperature-Dependent Dissipation at Nonequili-brium in Atomically Thin Clean-Limit Superconductors. *Nano Lett.* **2021**, *21*, 583−589.

(9) Cao, Y.; Fatemi, V.; Fang, S.; Watanabe, K.; Taniguchi, T.; Kaxiras, E.; Jarillo-Herrero, P. Unconventional superconductivity in magic-angle graphene superlattices. *Nature* **2018**, *556*, 43−50.

(10) Sajadi, E.; Palomaki, T.; Fei, Z.; Zhao, W.; Bement, P.; Olsen, C.; Luescher, S.; Xu, X.; Folk, J. A.; Cobden, D. H. Gate-induced superconductivity in a monolayer topological insulator. *Science* **2018**, *362*, 922−925.

(11) Fatemi, V.; Wu, S.; Cao, Y.; Bretheau, L.; Gibson, Q. D.; Watanabe, K.; Taniguchi, T.; Cava, R. J.; Jarillo-Herrero, P. Electrically tunable low-density superconductivity in a monolayer topological insulator. *Science* **2018**, *362*, 926−929.

(12) Huang, L.; McCormick, T. M.; Ochi, M.; Zhao, Z.; Suzuki, M.-T.; Arita, R.; Wu, Y.; Mou, D.; Cao, H.; Yan, J.; et al. Spectroscopic evidence for a type II Weyl semimetallic state in MoTe 2. *Nat. Mater.* **2016**, *15*, 1155−1160.

(13) Zhou, Q.; Rhodes, D.; Zhang, Q. R.; Tang, S.; Schönemann, R.; Balicas, L. Hall effect within the colossal magnetoresistive semi-metallic state of **MoTe**$_2$. *Phys. Rev. B: Condens. Matter Mater. Phys.* **2016**, *94*, 121101.

(14) Mandal, M.; Marik, S.; Sajilesh, K. P.; Arushi Singh, D.; Chakraborty, J.; Ganguli, N.; Singh, R. P. Enhancement of the superconducting transition temperature by Re doping in Weyl semimetal MoTe$_2$. *Physical Review Materials* **2018**, *2*, 094201.

(15) Qi, Y.; et al. Superconductivity in Weyl semimetal candidate MoTe2. *Nat. Commun.* **2016**, *7*, 11038.

(16) Cui, J.; Li, P.; Zhou, J.; He, W.-Y.; Huang, X.; Yi, J.; Fan, J.; Ji, Z.; Jing, X.; Qu, F.; et al. Transport evidence of asymmetric spin-orbit coupling in few-layer superconducting 1 T d-MoTe 2. *Nat. Commun.* **2019**, *10* (1), 2044.

(17) Naylor, C. H.; Parkin, W. M.; Ping, J.; Gao, Z.; Zhou, Y. R.; Kim, Y.; Streller, F.; Carpick, R. W.; Rappe, A. M.; Drndić, M.; Kikkawa, J. M.; Johnson, A. T. C. Monolayer Single-Crystal 1T'-MoTe2 Grown by Chemical Vapor Deposition Exhibits Weak Antilocalization Effect. *Nano Lett.* **2016**, *16*, 4297−4304.

(18) Yu, Y.; Ma, L.; Cai, P.; Zhong, R.; Ye, C.; Shen, J.; Gu, G. D.; Chen, X. H.; Zhang, Y. High-temperature superconductivity in monolayer Bi 2 Sr 2 CaCu 2 O 8+ δ. *Nature* **2019**, *575*, 156−163.

(19) Zhao, S. F.; Poccia, N.; Panetta, M. G.; Yu, C.; Johnson, J. W.; Yoo, H.; Zhong, R.; Gu, G.; Watanabe, K.; Taniguchi, T.; et al. Sign-Reversing Hall Effect in Atomically Thin High-Temperature Bi 2.1 Sr 1.9 CaCu 2.0 O 8+ δ Superconductors. *Phys. Rev. Lett.* **2019**, *122*, 247001.

(20) Liao, M.; Zang, Y.; Guan, Z.; Li, H.; Gong, Y.; Zhu, K.; Hu, X.-P.; Zhang, D.; Xu, Y.; Wang, Y.-Y.; et al. Superconductivity in few-layer stanene. *Nat. Phys.* **2018**, *14*, 344−348.

(21) Adams, P. W.; Nam, H.; Shih, C.-K.; Catelani, G. Zeeman-limited superconductivity in crystalline Al films. *Phys. Rev. B: Condens. Matter Mater. Phys.* **2017**, *95*, 094520.

(22) Ozer, M. M. *Growth and Superconductivity of Pb and Pb-Bi Alloys in the Quantum Regime.* Ph.D. thesis, The University of Tennessee, Knoxville, 2006.

(23) Edelberg, D.; et al. Approaching the Intrinsic Limit in Transition Metal Diselenides via Point Defect Control. *Nano Lett.* **2019**, *19*, 4371−4379.

(24) Wang, D.; Smyser, K.; Rhodes, D.; Balicas, L.; Pasupathy, A.; Herman, I. P. Passivating 1T'-MoTe2 multilayers at elevated temperatures by encapsulation. *Nanoscale* **2017**, *9*, 13910−13914.

(25) Telford, E. J.; Benyamini, A.; Rhodes, D.; Wang, D.; Jung, Y.; Zangiabadi, A.; Watanabe, K.; Taniguchi, T.; Jia, S.; Barmak, K.; Pasupathy, A. N.; Dean, C. R.; Hone, J. Via Method for Lithography Free Contact and Preservation of 2D Materials. *Nano Lett.* **2018**, *18*, 1416−1420.

(26) Dawson, W. G.; Bullett, D. W. Electronic structure and crystallography of MoTe$_2$ and WTe$_2$. *J. Phys. C: Solid State Phys.* **1987**, *20*, 6159.

(27) He, R.; Zhong, S.; Kim, H. H.; Ye, G.; Ye, Z.; Winford, L.; McHaffie, D.; Rilak, I.; Chen, F.; Luo, X.; Sun, Y.; Tsen, A. W. Dimensionality-driven orthorhombic MoTe$_2$ at room temperature. *Phys. Rev. B: Condens. Matter Mater. Phys.* **2018**, *97*, 041410.

(28) Shi, L.-k.; Song, J. C. W. Symmetry, spin-texture, and tunable quantum geometry in a WTe$_2$ monolayer. *Phys. Rev. B: Condens. Matter Mater. Phys.* **2019**, *99*, 035403.

(29) Keum, D. H.; Cho, S.; Kim, J. H.; Choe, D.-H.; Sung, H.-J.; Kan, M.; Kang, H.; Hwang, J.-Y.; Kim, S. W.; Yang, H.; Chang, K. J.; Lee, Y. H. Bandgap opening in few-layered monoclinic MoTe$_2$. *Nat. Phys.* **2015**, *11*, 482−486.

(30) Tang, S.; Zhang, C.; Jia, C.; Ryu, H.; Hwang, C.; Hashimoto, M.; Lu, D.; Liu, Z.; Devereaux, T. P.; Shen, Z.-X.; Mo, S.-K. Electronic structure of monolayer 1T'-MoTe$_2$ grown by molecular beam epitaxy. *APL Mater.* **2018**, *6*, 026601.

(31) Pawlik, A.-S.; Aswartham, S.; Morozov, I.; Knupfer, M.; Büchner, B.; Efremov, D. V.; Koitzsch, A. Thickness dependent electronic structure of exfoliated mono- and few-layer 1T'-MoTe$_2$. *Physical Review Materials* **2018**, *2*, 104004.

(32) Park, J. C.; Jung, E.; Lee, S.; Hwang, J.; Lee, Y. H. Evidence of shallow band gap in ultrathin 1T'-MoTe$_2$ via infrared spectroscopy. *Phys. Rev. B: Condens. Matter Mater. Phys.* **2020**, *101*, 235434.

(33) Tinkham, M. *Introduction to Superconductivity*, 2nd ed.; Dover Publications: Mineola, NY, 2004.

(34) Guguchia, Z.; et al. Signatures of the topological s + - superconducting order parameter in the type-II Weyl semimetal T d-MoTe2. *Nat. Commun.* **2017**, *8*, 1082.

(35) Ziman, J. M. *Electrons and phonons: the theory of transport phenomena in solids*; Oxford University Press: Oxford, 2001.

(36) Simonin, J. Surface term in the superconductive Ginzburg-Landau free energy: Application to thin films. *Phys. Rev. B: Condens. Matter Mater. Phys.* **1986**, *33*, 7830−7832.

(37) Carbotte, J. P. Properties of boson-exchange superconductors. *Rev. Mod. Phys.* **1990**, *62*, 1027−1157.

(38) Huang, Y. N.; Pickett, W. E. Electronic coupling between a FeSe monolayer film and SrTiO$_3$ substrate. *Phys. Rev. B: Condens. Matter Mater. Phys.* **2017**, *95*, 165107.

(39) Yang, Y.; Fang, S.; Fatemi, V.; Ruhman, J.; Navarro-Moratalla, E.; Watanabe, K.; Taniguchi, T.; Kaxiras, E.; Jarillo-Herrero, P. Enhanced superconductivity upon weakening of charge density wave transport in 2*H*-TaS$_2$ in the two-dimensional limit. *Phys. Rev. B: Condens. Matter Mater. Phys.* **2018**, *98*, 035203.

(40) Paul, S.; Karak, S.; Mandal, M.; Ram, A.; Marik, S.; Singh, R.; Saha, S. Tailoring the phase transition and electron-phonon coupling in 1T'- MoTe2 by charge doping: A Raman study. *Phys. Rev. B: Condens. Matter Mater. Phys.* **2020**, *102*, 054103.

(41) Beams, R.; Cançado, L. G.; Krylyuk, S.; Kalish, I.; Kalanyan, B.; Singh, A. K.; Choudhary, K.; Bruma, A.; Vora, P. M.; Tavazza, F.; et al. Characterization of few-layer 1T' MoTe2 by polarization-resolved second harmonic generation and Raman scattering. *ACS Nano* **2016**, *10*, 9626−9636.

(42) Heikes, C.; Liu, I.-L.; Metz, T.; Eckberg, C.; Neves, P.; Wu, Y.; Hung, L.; Piccoli, P.; Cao, H.; Leao, J.; et al. Mechanical control of crystal symmetry and superconductivity in Weyl semimetal MoTe 2. *Physical Review Materials* **2018**, *2*, 074202.

(43) Rhodes, D.; et al. Bulk Fermi surface of the Weyl type-II semimetallic candidate γ -MoTe$_2$. *Phys. Rev. B: Condens. Matter Mater. Phys.* **2017**, *96*, 165134.

(44) Luo, X.; Chen, F. C.; Zhang, J. L.; Pei, Q. L.; Lin, G. T.; Lu, W. J.; Han, Y. Y.; Xi, C. Y.; Song, W. H.; Sun, Y. P. Td-MoTe2: A possible topological superconductor. *Appl. Phys. Lett.* **2016**, *109*, 102601.

(45) Navarro-Moratalla, E.; Island, J. O.; Mañas-Valero, S.; Pinilla-Cienfuegos, E.; Castellanos-Gomez, A.; Quereda, J.; Rubio-Bollinger, G.; Chirolli, L.; Silva-Guillén, J. A.; Agraït, N.; Steele, G. A.; Guinea, F.; Zant, H. S. J. v. d.; Coronado, E. Enhanced superconductivity in atomically thin TaS$_2$. *Nat. Commun.* **2016**, *7*, 11043.

(46) Xie, Y.-M.; Zhou, B. T.; Law, K. T. Spin-Orbit-Parity-Coupled Superconductivity in Topological Monolayer WTe$_2$. *Phys. Rev. Lett.* **2020**, *125*, 107001.

(47) Wang, Y.; Xiao, J.; Zhu, H.; Li, Y.; Alsaid, Y.; Fong, K. Y.; Zhou, Y.; Wang, S.; Shi, W.; Wang, Y.; Zettl, A.; Reed, E. J.; Zhang, X. Structural phase transition in monolayer MoTe$_2$ driven by electro-static doping. *Nature* **2017**, *550*, 487−491.

(48) Duerloo, K.-A. N.; Li, Y.; Reed, E. J. Structural phase transitions in two-dimensional Mo- and W-dichalcogenide monolayers. *Nat. Commun.* **2014**, *5*, 4214.

(49) Kim, H.-J.; Kang, S.-H.; Hamada, I.; Son, Y.-W. Origins of the structural phase transitions in MoTe$_2$ and WTe$_2$. *Phys. Rev. B: Condens. Matter Mater. Phys.* **2017**, *95*, 180101.

(50) Wang, W.; Kim, S.; Liu, M.; Cevallos, F.; Cava, R.; Ong, N. Evidence for an edge supercurrent in the Weyl superconductor MoTe2. *Science* **2020**, *368*, 534−537.